particles

MDPI

Article

Effect of the Coulomb Interaction on Nuclear Deformation and Drip Lines

Kenta Hagihara [1,*], Takashi Nakatsukasa [2,3,4] and Nobuo Hinohara [2,3]

[1] Degree Programs in Pure and Applied Sciences, University of Tsukuba, Tsukuba 305-8571, Japan
[2] Center for Computational Sciences, University of Tsukuba, Tsukuba 305-8577, Japan
[3] Institute of Pure and Applied Sciences, University of Tsukuba, Tsukuba 305-8571, Japan
[4] RIKEN Nishina Center, Wako 351-0198, Japan
* Correspondence: hagihara@nucl.ph.tsukuba.ac.jp

Abstract

Nuclei are self-bound systems in which the strong interaction (nuclear force) plays a dominant role, and the isospin is approximately a good quantum number. The isospin symmetry is primarily violated by electromagnetic interactions, namely Coulomb interactions among protons, the effects of which need be studied to understand the importance of the isospin symmetry. We investigate the effect of the Coulomb interaction on nuclear properties, especially quadrupole deformation and neutron drip line, utilizing the density functional method, which provides a universal description of nuclear systems in the entire nuclear chart. We carry out calculations of even–even nuclei with a proton number of $2 \leq Z \leq 60$. The results show that the Coulomb interaction plays a significant role in enhancing quadrupole deformation across a wide range of nuclei. We also find that, after including the Coulomb interaction, some nuclei near the neutron drip line become stable against two-neutron emissions, resulting in a shift in the drip line towards larger neutron numbers.

Keywords: energy density functional theory; Hartree–Fock–Bogoliubov theory; Coulomb interaction; quadrupole deformation; neutron drip line



Academic Editor: Theocharis Kosmas

Received: 30 April 2025
Revised: 9 July 2025
Accepted: 11 July 2025
Published: 24 July 2025

Citation: Hagihara, K.; Nakatsukasa, T.; Hinohara, N. Effect of the Coulomb Interaction on Nuclear Deformation and Drip Lines. *Particles* **2025**, *8*, 72. https://doi.org/10.3390/particles8030072

Copyright: © 2025 by the authors. Licensee MDPI, Basel, Switzerland. This article is an open access article distributed under the terms and conditions of the Creative Commons Attribution (CC BY) license (https://creativecommons.org/licenses/by/4.0/).

1. Introduction

1.1. Basic Properties of Nuclei

Nuclei are composed of two types of fermions, neutrons and protons, which are often regarded as identical particles (called "nucleons") with different isospins T_z. The number of nucleons (the sum of the proton and neutron numbers) is the mass number A. The reason large nuclei with $A > 300$ do not exist in nature is due to the repulsive Coulomb interaction among protons, which is the main subject of the present paper.

There are well-known properties of nuclei, such as the saturation density of nuclei ($\rho_0 \approx 0.16$ fm^{-3}), constant binding energy per nucleon ($B/A \approx 8$ MeV), nucleon's mean free path which is larger than the nuclear size, and the magic number of neutrons and protons (2, 8, 20, 28, 50, 82, ...) [1,2]. It is also known that the shell structure may be significantly changed in neutron-rich unstable nuclei, which produces new magic numbers, such as 16, 32, and 34 [3]. Nuclear shapes are also of great interest, and have been studied extensively in the past [4]. The shape coexistence and isomerism have also been popular topics in recent nuclear structure studies [5–8]. Collective motion associated with the shape degrees of freedom can appear at low energies due to the nuclear property of an

approximately constant B/A. This implies that a nucleus can be divided into two fragments without a substantial energy cost.Thus, it is relatively free for transformation into different shapes. Nuclear deformation is an example of spontaneous breaking of rotational symmetry in finite quantum many-body systems [9–11]. A variety of nuclear shapes are present in the nuclei, including octupole shapes, which also violate parity symmetry. Among these, the axially symmetric quadrupole deformation is the most common shape in nuclei [2], which will be discussed in the following sections.

1.2. Energy Density Functional Method

It is still difficult to directly solve the Schrödinger equation for finite nuclei with many nucleons, despite the recent significant progress in the ab initio calculations for the nuclear structure, based on various techniques for quantum many-body systems, such as the Monte-Carlo method [12,13], the coupled-cluster method [14], the self-consistent Green's function method [15], and the in-medium similarity renormalization group [16,17]. This is partially due to the singular, complicated, and many-body characters of the nuclear force [18–21], and the treatment of the center-of-mass motion for self-bound systems. Among many alternative methods, energy density functional (EDF) theory, which we use in this study, is one of the most powerful tools [11,22,23]. In nuclear physics, this approach is often used along with mean-field theory for density-dependent interactions, where each nucleon moves independently in an average potential. This is known as the density-dependent Hartree–Fock (DDHF) method [24]. DDHF was originally proposed by Negele and coworkers to improve the results of the Brückner Hartree–Fock calculations. Using local density approximation, the method results in the energy density functional $\mathcal{H}(\mathbf{r})$ which is a functional of local density, kinetic density, spin-orbit density, etc. Then, the variation for the total energy, $\delta \int \mathcal{H}(\mathbf{r}) d\mathbf{r} = 0$, leads to equations practically identical to those of the Kohn–Sham equations in density functional theory [25,26]. They succeeded in achieving a quantitative description for nuclei in a wide mass range [27]. It should be emphasized here that, in contrast with the electrons in atoms and molecules, nuclei have no external potential to bind nucleons. The nucleons are bound by a potential created by the nucleons themselves. In the nuclear EDF method, we should consider center-of-mass corrections, especially in studies of light nuclei.

1.3. Electromagnetic Interaction in Nuclei

Electromagnetic force plays a crucial role in many nuclear phenomena. For instance, alpha decay is described by quantum tunneling, in which an alpha particle travels through the Coulomb barrier potential [28]. It is also responsible only a finite number of species of elements existing on Earth. The repulsive Coulomb force among protons disfavors nuclei with large Z, which eventually leads to instability against nuclear fission [29]. ^{238}U is known as the heaviest "stable" nucleus on Earth. In fact, ^{238}U is unstable with respect to the alpha decay; however, due to their extremely long lifetime, uranium and similarly long-lived isotopes are sometimes categorized as "stable" nuclei.

The liquid drop model is one of the most successful nuclear models to represent the saturation property [30]. It is based on the classical liquid drop picture that always favors the spherical shape. Therefore, the deformed shape in the ground state of a nucleus is a consequence of the quantum mechanical effect, which is often referred to as "shell energy" or "shell correction" [31]. However, one may expect that the magnitude of the deformation is influenced by the Coulomb interaction, because Coulomb energy favors a non-spherical shape [1,32].

Another prominent electromagnetic effect can be found in the position of the proton drip line. The liquid drop model has a symmetry-energy term that favors nuclei with equal neutrons and protons, $N = Z$. However, there are no stable $N = Z$ nuclei beyond ^{40}Ca [33]. If the isospin symmetry is exact, the nuclear chart should be symmetric with respect to the $N = Z$ line. In reality, the $N - Z$ symmetry of the nuclear chart is significantly violated, and the proton drip line is located at $N > Z$ for heavy nuclei with $A > 100$. This is a trivial effect on the proton drip line. In this paper, we show a possible nontrivial Coulomb effect on the neutron drip line.

1.4. Scope of the Present Paper

We perform numerical calculations based on the Skyrme EDF. In addition, we perform calculations neglecting the Coulomb interaction. This makes it possible to estimate the effect of the Coulomb interaction on the nuclear properties. In this paper, we focus our discussion on changes in the quadrupole deformation and position of the neutron drip line.

2. Hartree–Fock–Bogoliubov Theory

Hartree–Fock–Bogoliubov (HFB) theory [11,23,32] is a powerful tool to treat many-body systems, in which the mean-field effects are dominant in both the particle–hole and particle–particle (hole–hole) channels. The HFB equation, derived by minimizing the EDF $E[\rho, \kappa]$, where ρ and κ are the particle and pair densities, respectively, can be solved by diagonalizing the HFB Hamiltonian. The solutions provide the Bogoliubov transformation to define quasi-particles $(\alpha_k, \alpha_k^\dagger)$ and their energies E_k. The quasi-particle energies have a gap, $E_k > \Delta$, when the system is in the superfluid phase.

Starting from a nuclear EDF $E[\rho, \kappa]$, the HFB equation is given in the form of the eigenvalue equation.

$$\begin{pmatrix} h - \lambda & \Delta \\ -\Delta^* & -(h - \lambda)^* \end{pmatrix} \begin{pmatrix} U_k \\ V_k \end{pmatrix} = E_k \begin{pmatrix} U_k \\ V_k \end{pmatrix}, \tag{1}$$

where

$$h_{nn'} \equiv \frac{\delta E}{\delta \rho_{n'n}}, \qquad \Delta_{nn'} \equiv \frac{\delta E}{\delta \kappa^*_{nn'}}, \tag{2}$$

and λ is the Fermi energy (chemical potential) to restrict the average number of particles. In the HFB method, the wave function of the ground state $|\phi\rangle$ is defined as the quasi-particle vacuum $\alpha_k |\phi\rangle = 0$, where the quasi-particle creation and annihilation operators $(\alpha, \alpha^\dagger)$ are connected to the particle creation and annihilation operators $(c, c^\dagger)$ via a unitary transformation, namely Bogoliubov transformation

$$\alpha_k = \sum_n (U^*_{nk} c_n + V^*_{nk} c_n^\dagger), \quad \alpha_k^\dagger = \sum_n (U_{nk} c_n^\dagger + V_{nk} c_n^\dagger). \tag{3}$$

In terms of the quasi-particle wave functions (U, V), the one-body density matrix ρ and the pair density κ are given as

$$\rho_{nn'} = \langle \phi | \, c_{n'}^\dagger c_n \, | \phi \rangle = (V^* V^T)_{nn'}, \quad \kappa_{nn'} = \langle \phi | \, c_{n'} c_n \, | \phi \rangle = (V^* U^T)_{nn'}. \tag{4}$$

Since the HFB Hamiltonian, the matrix on the left-hand side of Equation (1), depends on densities ρ and κ, we iteratively solve the equation until self-consistency is achieved.

In the present paper, we discuss the axial quadrupole deformation which is characterized by the following deformation parameter

$$\beta_2 = \frac{\sqrt{\pi}}{5}\frac{\langle \hat{Q}_2 \rangle}{A\langle r^2 \rangle}, \tag{5}$$

$$\hat{Q}_l = r^l Y_{l0}(\theta, \phi) = \sqrt{\frac{2l+1}{4\pi}} r^l P_l(\cos\theta). \tag{6}$$

The quasi-particle states and energies characterize the excitation properties of the superfluid system [32]. For a numerical purpose and physical interpretation, it is sometimes convenient to define the canonical single-particle states and their energies. The canonical single-particle states $d_i^\dagger$ are defined as those that diagonalize the density matrix ρ.

$$d_i^\dagger = \sum_n \phi_{ni} c_n^\dagger , \qquad \sum_{n'} \rho_{nn'} \phi_{n'i} = v_i^2 \phi_{ni}. \tag{7}$$

The eigenvalues $v_i^2 \geq 0$ correspond to the occupation number in the Bardeen–Cooper–Schrieffer (BCS) theory, although the canonical states i are not the energy eigenstates. The canonical single-particle energies e_i are defined by the expectation value of h in Equation (2); $e_i \equiv \langle \phi_i | h | \phi_i \rangle = \sum_{nn'} \phi_{ni}^* h_{nn'} \phi_{n'i}$.

3. Results

Numerical calculations are performed using an open source code HFBTHO [34]. We carried out a systematic calculation for even–even nuclei with $Z = 2 - 60$ using the SLy4 parameter set of the Skyrme functional that includes the density dependent term [35] with a mixed-type pairing. The self-consistent HFB equations are solved with the spherical harmonic oscillator basis of 20 major shells, namely, all the harmonic-oscillator single-particle states with the harmonic oscillator quanta of $N_{\rm sh} = 0, \ldots, 20$. The initial states of the iteration are set to have seven different quadrupole deformations with $\beta_2 = -0.3, -0.2, -0.1, \ldots,$ and 0.3. At the beginning of the self-consistent procedure, we performed the HFB calculation with a constraint on the quadrupole deformation. After 10 iterations, the constraint was released to find an optimal deformation. Comparing the converged energies with the different initial states, we define the ground state with the minimum energy among them. Using the ground-state wave function, we obtained quantities such as total energy, quadrupole deformation, and canonical single-particle energies. Then, we repeated the same calculation neglecting the Coulomb interaction among protons, to study the electromagnetic effect on the nuclear structure.

It should be noted that similar systematic calculations of nuclear deformation over the entire nuclear chart have been performed [36–38]. For instance, Stoitsov et al. [38], who developed the HFBTHO code, reported the results of the systematic calculation. They adopted three initial states with prolate, oblate, and spherical shapes to start the calculation. We used seven initial states between $\beta = -0.3$ and 0.3, although the final results are almost identical to their results [38].

3.1. Quadrupole Deformation

We show the results for the calculated quadrupole deformation β_2 for the cases where the Coulomb interaction is present and absent in Figures 1 and 2, respectively.

In the plot, we show nuclei with positive two-neutron-separation energy $S_{2n}(Z, N) = BE(Z, N+2) - BE(Z, N) > 0$, where BE expresses the binding energy. Those with the negative separation energy indicate that they are unbound.

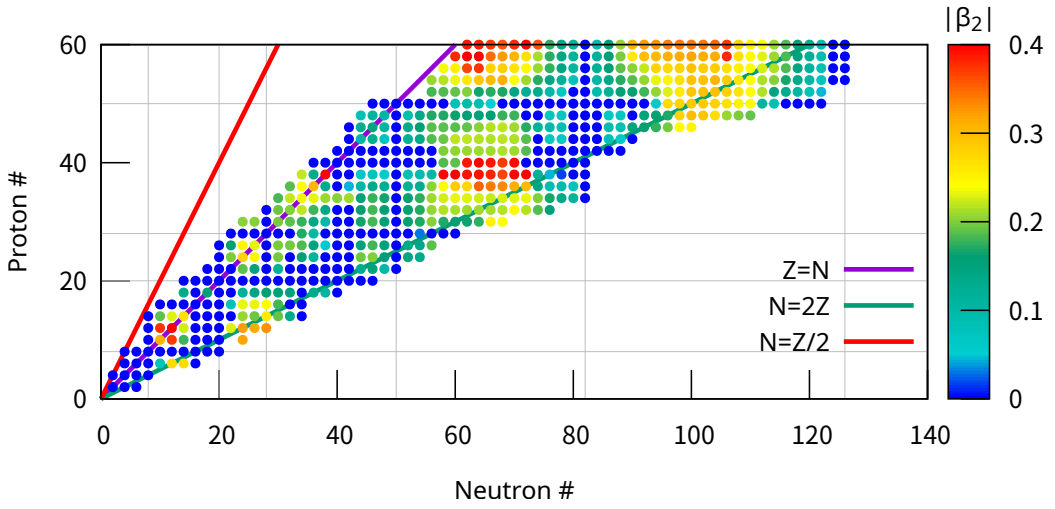


Figure 1. Deformation parameter $|\beta_2|$ of the calculated ground states of even–even nuclei with the SLy4 EDF including the Coulomb EDF. Those with positive two-nucleon separation energies (negative Fermi energy) are shown. The prolate and oblate shapes are not distinguished. The lines of $N = Z$, $N = 2Z$, and $Z = 2N$ are shown for reference. The observed trend—that nuclei with magic numbers of nucleons are spherical, while those in the region of $Z = 40$ and $N = 60 - 80$ exhibit larger deformation—is consistent with other studies of nuclear quadrupole deformation [39].

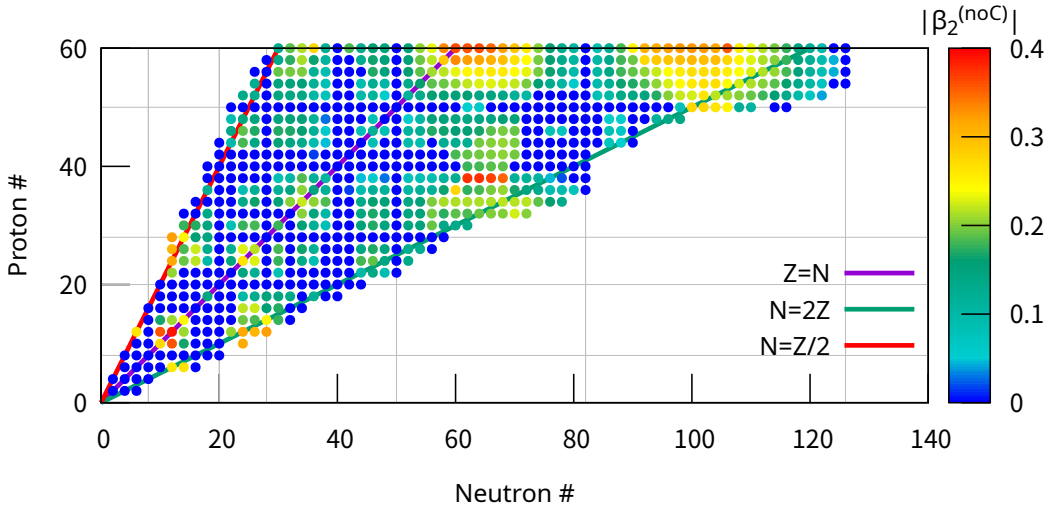


Figure 2. Same as Figure 1 but calculated without the Coulomb interaction, $|\beta_2^{(\mathrm{noC})}|$.

Although nuclei in the proton-rich side become unbound because of the Coulomb energy, for most nuclei, the spherical (deformed) nuclei stays spherical (deformed) regardless of the presence of the Coulomb interaction. This confirms our understanding of the nuclear deformation: The classical liquid drop always favors the sphericity, but the quantum shell effects drive the nucleus to be deformed [31]. Since the shell structure is mainly determined by the nuclear force (strong interaction), we expect that electromagnetic interactions provide only minor contributions to shell effects. The dominant role of the nuclear force on the shell structure is evidenced by the existence of the same magic numbers for protons and neutrons.

The Coulomb interaction plays a minor role in the determination of whether the nucleus is deformed or spherical. However, it influences the magnitude of deformation. In a general trend, the Coulomb interaction enhances the quadrupole deformation, as shown in Figure 3, in which we show $\delta|\beta_2|$, the difference in $|\beta_2|$ between those with and without the Coulomb interaction. The blank spots are spherical nuclei which keep the sphericity

in both calculations. A significant change in the deformation is caused by the shape coexistence (multiple potential-energy minima). The inclusion of the Coulomb interaction changes the ordering in energy of the potential local minima, which leads to a jump in the location of the absolute minimum. This is seen in many of the Zr isotopes ($Z = 40$) with $N = 60 - 70$. Nevertheless, we find no nuclei with $\delta|\beta_2| < 0$ in Figure 3, which is natural since the Coulomb energy favors a larger deformation. It should be noted that the superposition of different shapes is often required for such cases with approximately degenerate multiple potential minima.

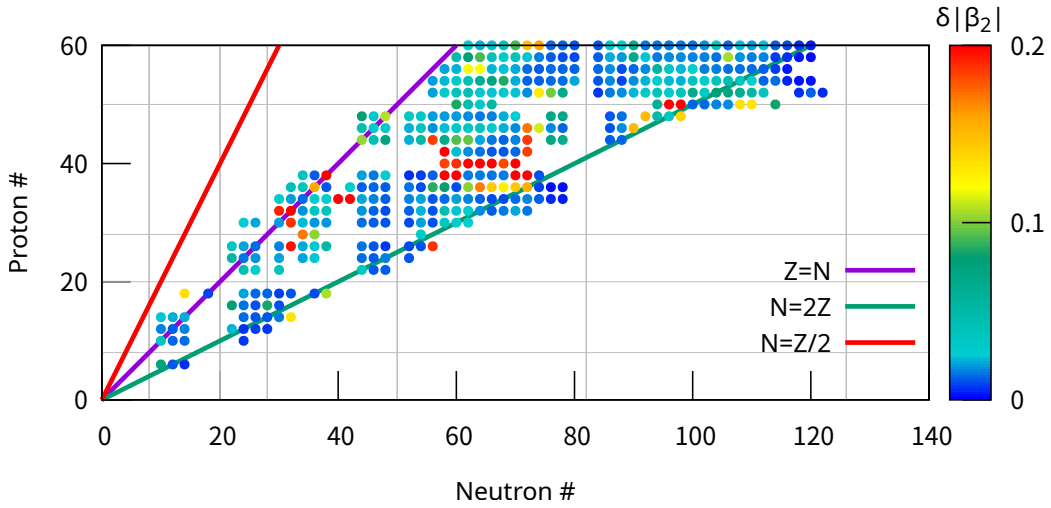


Figure 3. Difference in deformation $|\beta_2|$ between those calculated with and without the Coulomb interaction; $\delta|\beta_2| \equiv |\beta_2| - |\beta_2^{(\mathrm{noC})}|$ The blank spaces indicate the spherical nuclei with $\delta|\beta_2| = 0$.

3.2. Neutron Drip Line

The electromagnetic interaction makes many nuclei unstable against proton emission [40]. This is clearly seen in Figures 1 and 2. A large number of nuclei in the proton-rich side of Figure 2 are absent in Figure 1, becoming unbound with respect to the (two-)proton emission. As the Coulomb barrier may hold unbound protons for a while, some of them may be metastable proton emitters. In addition, the Coulomb interaction makes heavy nuclei unstable against the fission and the alpha decay [41]. These are well-known and naively expected effects of the electromagnetic interaction for nuclei.

In contrast, the results seen on the neutron-rich side are somewhat interesting. The repulsive Coulomb interaction provides an additional binding effect to neutron-rich nuclei near the drip line. Some unbound nuclei calculated with only the nuclear part of the EDF become bound by including the Coulomb interaction among protons. The Coulomb interaction between two protons has a repulsive nature, thus, the total binding energy should always be reduced. However, the position of the neutron drip line is determined by the two-neutron separation energy, which is the difference in the binding energy between N and $N - 2$ neutron systems (The odd-even mass difference in nuclei predicts the mass difference between even-N and odd-N of order of 1 MeV, which is significantly larger than the calculated two-neutron separation energy near the drip line.). The two-neutron separation energy is well approximated by $-2\lambda_n$, where λ_n is the neutron Fermi energy in Equation (1).

Figure 4 shows that 29 bound nuclei in Figure 1 are actually unbound in Figure 2 without the Coulomb interaction. We see that these contain both spherical and deformed nuclei, which means that it is not due to a gain in the Coulomb energy caused by the deformation.

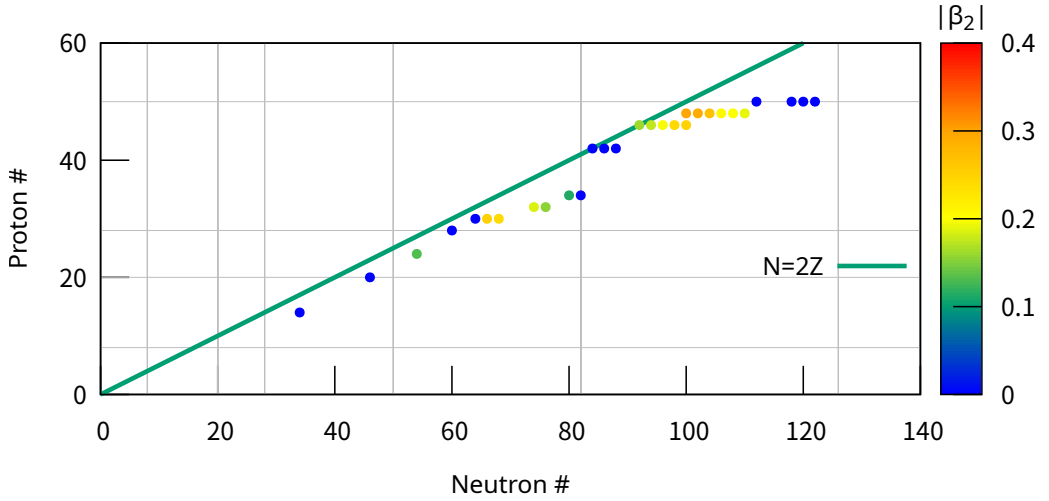


Figure 4. Nuclei bound by the inclusion of the Coulomb interaction. In other words, those exist in Figure 1 but are missing in Figure 2. The color indicates $|\beta_2|$.

3.3. Canonical Single-Particle Energy of Neutrons

To examine the mechanism of the shift of the neutron drip line, we investigate the canonical single-particle energies e_i of both protons and neutrons. The Coulomb interaction trivially increases the protons' single-particle energies. In other words, *the protons become less bound*. In contrast, the single-particle orbits of weakly bound neutrons, shown in Figure 5 for ^{170}Sn, decrease their energies. *The neutrons are more bound.* The ^{170}Sn nucleus has a spherical shape and is one of the nuclei that are bound only when the Coulomb interaction is included. The inclusion of the Coulomb interaction lowers the energies by several hundreds of keV, which affects the Fermi energy λ_n, leading to an increase in neutron separation energy.

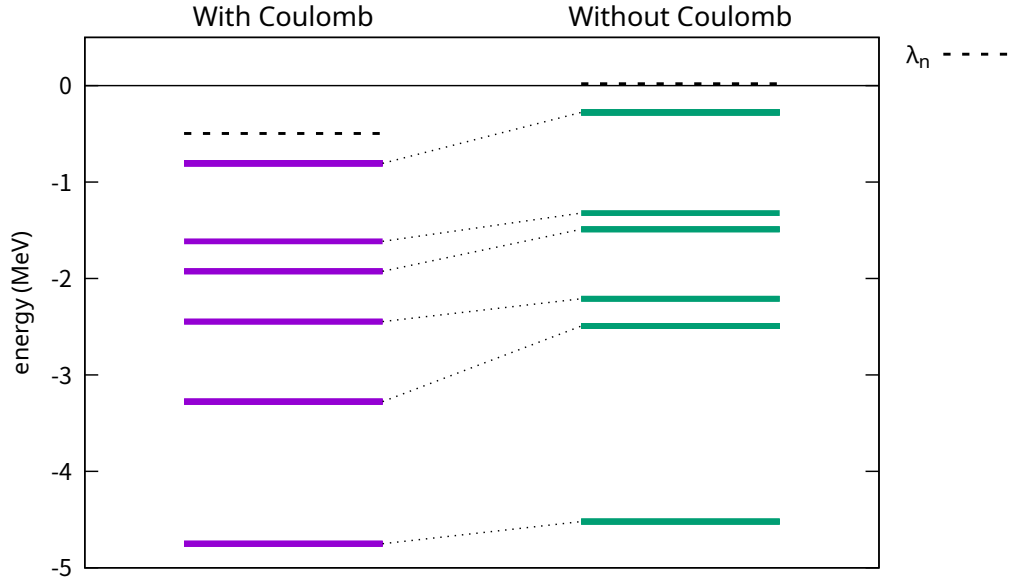


Figure 5. Canonical single-particle energies for neutrons in ^{170}Sn, including and excluding the Coulomb interaction in the left (magenta line) and right panel (green line), respectively. The orbits are, from top to bottom, $1i_{13/2}$, $3p_{1/2}$, $2f_{5/2}$, $3p_{3/2}$, $1h_{9/2}$, and $2f_{7/2}$. The neutron Fermi energy (chemical potential) is shown by the black dashed line.

The Coulomb interaction cannot increase the depth of the attractive potential for neutrons. In fact, we find the opposite effect, namely, a reduction in the neutron potential depth. We think the change in λ_n cannot be explained in the scope of classical mechanics. It is a quantum mechanical effect to shift the neutron energies through a change in the proton density distribution. Due to the repulsive character of the Coulomb interaction, the proton density distribution slightly expands, which reduces the potential depth for neutrons, but expands the potential range (nuclear radius). For single-particle energies near the bottom of the potential, the former effect is dominant, and we find that the single-particle energies for neutrons increase. In contrast, near the threshold $e_i \approx 0$, the latter effect dominates, thus, the kinetic energy decreases because of the spread of the single-particle wave functions. This is a quantum mechanical effect for fermions in a confined potential, associated with the uncertainty principle.

4. Conclusions

We carried out the calculations using the Skyrme SLy4 EDF with and without the Coulomb EDF for nuclei with $Z = 2 - 60$, to find out the electromagnetic effect in nuclei. In this paper, we focus our discussion on the change in the quadrupole deformation and the particle binding. In many deformed nuclei, the quadrupole deformation is enhanced by the Coulomb interaction. On the other hand, most of the spherical nuclei stay spherical regardless of the presence of the Coulomb interaction among protons. This confirms that the quantum shell effects determine whether the nucleus is deformed or not.

The Coulomb interaction affects not only the position of the proton drip line, but also that of the neutron drip line, especially for nuclei with $Z \gtrsim 40$. The neutron drip line moves to larger neutron numbers, and the region of the neutron-rich nuclei is extended. This is unexpected because the Coulomb interaction in the nucleus is repulsive and acts only among protons. It seems to be due to a quantum mechanical effect: The repulsive interaction makes the nuclear size larger, which leads to a decrease in the kinetic energy of neutrons near the threshold. An investigation of the canonical single-particle energies reveals that the neutron energies near the threshold decrease with the inclusion of the Coulomb interaction.

In this paper, we treat the exchange term of the Coulomb in the Slater approximation [22]. However, we think that the calculation of the exact Coulomb exchange term does not affect the conclusion, because the magnitude of the exchange is significantly smaller than that of the direct term and the Coulomb effect discussed in the present paper is not directly associated with the exchange term. We expect that the electromagnetic effects are larger in the heavier systems, simply because the proton number Z and the Coulomb energy are larger. It is desired to extend the present study to expand the region of the investigation to rare-earth, actinide, and super-heavy nuclei. Studies in this direction are currently underway.

Author Contributions: Investigation, K.H.; writing—original draft preparation, K.H.; writing—review and editing, T.N. and N.H.; funding acquisition, T.N. and N.H. All authors have read and agreed to the published version of the manuscript.

Funding: This work is supported by JST ERATO Grant No. JPMJER2304, and KAKENHI Grant No. JP23K25864 and No. JP25K07312, Japan.

Data Availability Statement: The data presented in this study are available on request from the corresponding author.

Conflicts of Interest: The authors declare no conflicts of interest.

References

1. Bohr, A.; Mottelson, B.R. *Nuclear Structure*; W. A. Benjamin: New York, NY, USA, 1969; Volume I.
2. Bohr, A.; Mottelson, B.R. *Nuclear Structure*; W. A. Benjamin: New York, NY, USA, 1975; Volume II.
3. Li, J.J.; Margueron, J.; Long, W.H.; Van Giai, N. Magicity of neutron-rich nuclei within relativistic self-consistent approaches. *Phys. Lett. B* **2016**, *753*, 97–102. [CrossRef]
4. Åberg, S.; Flocard, H.; Nazarewicz, W. Nuclear Shapes in Mean Field Theory. *Annu. Rev. Nucl. Part. Sci.* **1990**, *40*, 439–528. [CrossRef]
5. Heyde, K.; Wood, J.L. Shape Coexistence in Atomic Nuclei. *Rev. Mod. Phys.* **2011**, *83*, 1467–1521. [CrossRef]
6. Gade, A.; Liddick, S.N. Shape Coexistence in Neutron-Rich Nuclei. *J. Phys. G: Nucl. Part. Phys.* **2016**, *43*, 024001. [CrossRef]
7. Leoni, S.; Fornal, B.; Bracco, A.; Tsunoda, Y.; Otsuka, T. Multifaceted character of shape coexistence phenomena in atomic nuclei. *Prog. Part. Nucl. Phys.* **2024**, *139*, 104119. [CrossRef]
8. Aprahamian, A.; Lee, K.; Lesher, S.R.; Bijker, R. The nature of 0+ excitations in deformed nuclei. *Prog. Part. Nucl. Phys.* **2025**, *143*, 104173. [CrossRef]
9. Alder, K.; Bohr, A.; Huus, T.; Mottelson, B.; Winther, A. Study of Nuclear Structure by Electromagnetic Excitation with Accelerated Ions. *Rev. Mod. Phys.* **1956**, *28*, 432–542. [CrossRef]
10. Nakatsukasa, T.; Matsuyanagi, K.; Matsuzaki, M.; Shimizu, Y.R. Quantal rotation and its coupling to intrinsic motion in nuclei. *Phys. Scr.* **2016**, *91*, 073008. [CrossRef]
11. Nakatsukasa, T.; Matsuyanagi, K.; Matsuo, M.; Yabana, K. Time-dependent density-functional description of nuclear dynamics. *Rev. Mod. Phys.* **2016**, *88*, 045004. [CrossRef]
12. Carlson, J.; Gandolfi, S.; Pederiva, F.; Pieper, S.C.; Schiavilla, R.; Schmidt, K.E.; Wiringa, R.B. Quantum Monte Carlo methods for nuclear physics. *Rev. Mod. Phys.* **2015**, *87*, 1067–1118. [CrossRef]
13. Gandolfi, S.; Lonardoni, D.; Lovato, A.; Piarulli, M. Atomic Nuclei From Quantum Monte Carlo Calculations With Chiral EFT Interactions. *Front. Phys.* **2020**, *8*, 117. [CrossRef]
14. Hagen, G.; Papenbrock, T.; Hjorth-Jensen, M.; Dean, D.J. Coupled-cluster computations of atomic nuclei. *Rep. Prog. Phys.* **2014**, *77*, 096302. [CrossRef] [PubMed]
15. Somà, V. Self-Consistent Green's Function Theory for Atomic Nuclei. *Front. Phys.* **2020**, *8*, 340. [CrossRef]
16. Hergert, H. A Guided Tour of ab initio Nuclear Many-Body Theory. *Front. Phys.* **2020**, *8*, 379. [CrossRef]
17. Miyagi, T. Nuclear radii from first principles. *Front. Phys.* **2025**, *13*, 1581854. [CrossRef]
18. Epelbaum, E.; Hammer, H.W.; Meißner, U.G. Modern theory of nuclear forces. *Rev. Mod. Phys.* **2009**, *81*, 1773–1825. [CrossRef]
19. Machleidt, R.; Entem, D. Chiral effective field theory and nuclear forces. *Phys. Rep.* **2011**, *503*, 1–75. [CrossRef]
20. Epelbaum, E.; Krebs, H.; Reinert, P. High-Precision Nuclear Forces From Chiral EFT: State-of-the-Art, Challenges, and Outlook. *Front. Phys.* **2020**, *8*, 98. [CrossRef]
21. Machleidt, R.; Sammarruca, F. Recent advances in chiral EFT based nuclear forces and their applications. *Prog. Part. Nucl. Phys.* **2024**, *137*, 104117. [CrossRef]
22. Vautherin, D.; Brink, D.M. Hartree-Fock Calculations with Skyrme's Interaction. I. Spherical Nuclei. *Phys. Rev. C* **1972**, *5*, 626–647. [CrossRef]
23. Bender, M.; Heenen, P.H.; Reinhard, P.G. Self-consistent mean-field models for nuclear structure. *Rev. Mod. Phys.* **2003**, *75*, 121–180. [CrossRef]
24. Negele, J.W. The mean-field theory of nuclear structure and dynamics. *Rev. Mod. Phys.* **1982**, *54*, 913–1015. [CrossRef]
25. Hohenberg, P.; Kohn, W. Inhomogeneous Electron Gas. *Phys. Rev.* **1964**, *136*, B864–B871. [CrossRef]
26. Kohn, W.; Sham, L.J. Self-consistent equations including exchange and correlation effects. *Phys. Rev.* **1965**, *140*, A1133–A1138. [CrossRef]
27. Negele, J.W.; Vautherin, D. Density-Matrix Expansion for an Effective Nuclear Hamiltonian. *Phys. Rev. C* **1972**, *5*, 1472–1493. [CrossRef]
28. Gamow, G. Zur Quantentheorie des Atomkernes. *Z. Phys.* **1928**, *51*, 204–212. [CrossRef]
29. Bohr, N.; Wheeler, J.A. The Mechanism of Nuclear Fission. *Phys. Rev.* **1939**, *56*, 426–450. [CrossRef]
30. Ragnarsson, I.; Nilsson, S.G. Nuclear fission and the liquid-drop model. In *Shapes and Shells in Nuclear Structure*; Cambridge University Press: Cambridge, UK, 1995. [CrossRef]
31. Brack, M.; Damgaard, J.; Jensen, A.S.; Pauli, H.C.; Strutinsky, V.M.; Wong, C.Y. Funny Hills: The Shell-Correction Approach to Nuclear Shell Effects and Its Applications to the Fission Process. *Rev. Mod. Phys.* **1972**, *44*, 320–405. [CrossRef]
32. Ring, P.; Schuck, P. *The Nuclear Many-Body Problems*; Texts and Monographs in Physics; Springer: New York, NY, USA, 1980.
33. Roeckl, E. Decay Studies of N~Z Nuclei. *Lect. Notes Phys.* **2004**, *651*, 223–261. [CrossRef]
34. Perez, R.N.; Schunck, N.; Lasseri, R.D.; Zhang, C.; Sarich, J. Axially deformed solution of the Skyrme–Hartree–Fock–Bogolyubov equations using the transformed harmonic oscillator basis (III) hfbtho (v3.00): A new version of the program. *Comput. Phys. Commun.* **2017**, *220*, 363–375. [CrossRef]

35. Chabanat, E.; Bonche, P.; Haensel, P.; Meyer, J.; Schaeffer, R. A Skyrme parametrization from subnuclear to neutron star densities. *Nucl. Phys. A* **1997**, *627*, 710–746. [CrossRef]
36. Robledo, L.M.; Rodríguez, T.R.; Rodríguez-Guzmán, R.R. Mean field and beyond description of nuclear structure with the Gogny force: A review. *J. Phys. G: Nucl. Part. Phys.* **2018**, *46*, 013001. [CrossRef]
37. Hirata, D.; Sumiyoshi, K.; Tanihata, I.; Sugahara, Y.; Tachibana, T.; Toki, H. A systematic study of even–even nuclei up to the drip lines within the relativistic mean field framework. *Nucl. Phys. A* **1997**, *616*, 438–445. [CrossRef]
38. Stoitsov, M.V.; Dobaczewski, J.; Nazarewicz, W.; Pittel, S.; Dean, D.J. Systematic study of deformed nuclei at the drip lines and beyond. *Phys. Rev. C* **2003**, *68*, 054312. [CrossRef]
39. Ebata, S.; Nakatsukasa, T. Octupole deformation in the nuclear chart based on the 3D Skyrme Hartree–Fock plus BCS model. *Phys. Scr.* **2017**, *92*, 064005. [CrossRef]
40. Delion, D.S.; Liotta, R.J.; Wyss, R. Systematics of Proton Emission. *Phys. Rev. Lett.* **2006**, *96*, 072501. [CrossRef]
41. Santhosh, K.P.; Biju, R.K.; Sahadevan, S. Spontaneous fission versus alpha radioactivity in heavy and super heavy nuclei. *Proc. Int. Symp. Nucl. Phys.* **2009**, *54*, 216–217.

Disclaimer/Publisher's Note: The statements, opinions and data contained in all publications are solely those of the individual author(s) and contributor(s) and not of MDPI and/or the editor(s). MDPI and/or the editor(s) disclaim responsibility for any injury to people or property resulting from any ideas, methods, instructions or products referred to in the content.